ECONOMIC GEOLOGY

RESEARCH UNIT

University of the Witwatersrand

Johannesburg

GOLD MINERALIZATION AT TURK MINE, ZIMBABWE: GEOCHEMICAL AND STATISTICAL INVESTIGATION OF THE HYDROTHERMALLY OVERPRINTED HOST ROCK

A. DZIGGEL, R. KLEMD and G. STEVENS

INFORMATION CIRCULAR No.327

GOLD MINERALIZATION AT TURK MINE, ZIMBABWE: GEOCHEMICAL AND STATISTICAL INVESTIGATION OF THE HYDROTHERMALLY OVERPRINTED HOST ROCK

ABSTRACT

The Turk Gold Mine, located in the northeastern part of the Bulawayo-Bubi greenstone belt (BBGB), occurs in a narrow intrashear corridor. The mineral assemblages of the metabasaltic country rock indicate greenschist-facies conditions, during which extensive hydrothermal alteration has produced the mineral assemblage carbonate + chlorite + plagioclase + quartz + opaque ± actinolite ± zoisite ± epidote. The different styles of alteration, such as carbonatization, chloritization, sericitization and silicification of the (ultra-) mylonitized wall rock, cannot be correlated unequivocally with the gold mineralization. Furthermore, these alteration types represent different geochemical processes, which predate the gold-mineralization. While the carbonatization and chloritization occur on a regional scale, sericitization is restricted to local structures within the highly deformed metabasalts. However, the precipitation of secondary quartz occurred during carbonatization. Gold-mineralization at the Turk Mine is synkinematic and took place in a brittle-ductile deformation regime under greenschist facies conditions. A statistically significant correlation between gold and arsenic as well as gold and sulphur indicate an association of gold with arsenopyrite and/or pyrite. Since the deposit is not characterized by a typical alteration halo, it is suggested that the gold-bearing fluids were either in chemical equilibrium with the altered wall rock or infiltrated the metabasalts at relatively low temperatures. Gold in the altered wall rock ($\bar{x}$ = 0,2 ppm) is enriched relative to average gold-concentrations of other Archaean greenstone belts ($\bar{x}$ = 10 ppb), while the investigated ore bodies have average gold-concentrations around 3 ppm. This gold deposit is, therefore, interpreted to have formed either as a result of dramatically inhomogeneous distribution of gold introduced during one hydrothermal event, or to be a consequence of secondary remobilization and concentration of gold introduced during an initial hydrothermal event.

oOo

GOLD MINERALIZATION AT TURK MINE, ZIMBABWE: GEOCHEMICAL AND STATISTICAL INVESTIGATION OF THE HYDROTHERMALLY OVERPRINTED HOST ROCK

CONTENTS

_____oOo_____

Published by the Economic Geology Research Unit
Department of Geology
University of the Witwatersrand
1 Jan Smuts Avenue
Johannesburg 2001
South Africa

ISBN 1-86838-240-0

GOLD MINERALIZATION AT TURK MINE, ZIMBABWE: GEOCHEMICAL AND STATISTICAL INVESTIGATION OF THE HYDROTHERMALLY OVERPRINTED HOST ROCK

INTRODUCTION

Most Zimbabwian gold production has been derived from lode deposits. These range from pervasively silicified and sulphidized schistose zones and shear zone vein arrays, to ribbon-textured and massive quartz-veins (Foster, 1989). Economic gold mineralization in Archaean greenstone belts is usually structurally controlled and occurs in metamorphosed Fe-rich mafic and/or sedimentary host rocks (e.g. Phillips & Groves, 1984; Groves, 1993). The immediate wall rocks of the gold-bearing veins reveal varying degrees of hydrothermal overprinting. The geochemical changes, such as potassium enrichment within the wall rocks, which are induced during the hydrothermal alteration, are often correlated with the Au-enrichment and can thus be used as an exploration tool (Boyle, 1979; Colvine et al., 1988). The aim of this paper is to demonstrate statistically, that geochemical changes during pervasive hydrothermal alteration events cannot unequivocally be correlated with the Au-enrichment at the Turk Mine in the Bulawayo-Bubi greenstone belt. This has important consequences for models of the formation of this deposit, strongly favouring at least two episodes of hydrothermal processes.

REGIONAL SETTING AND GEOLOGY OF THE TURK MINE AREA

The Turk Mine is situated in the northeastern part of the Bulawayo-Bubi greenstone belt in the southwestern part of the Zimbabwe craton. The BBGB is one of the largest late Archaean greenstone belts in Zimbabwe with an exposed area of about 4196 km^2 (Blenkinsop et al., 1997). Stratigraphically, the BBGB comprises a variably metamorphosed assemblage of ultramafic, mafic, intermediate and felsic volcanic and intrusive rocks with related volcanoclastics and other sediments, including banded iron formation (BIF) of predominantly Upper Bulawayan age (ca. 2.7 Ga, Fig. 1).

The greenstone belt is intruded by syn- to late-tectonic TTG granitoids and late- to post-tectonic granites and quartz-monzonites (Campbell & Pitfield, 1994). Previous geological investigations of the Bubi district and the Bulawayo district were undertaken by Macgregor et al. (1937) and Garson & Fimm (1995), respectively. To the end of 1991, the Turk Mine had produced 12619.33 kg gold. An overview of the structural framework of the Turk Mine was given by Campbell & Pitfield (1994), who classified the deposit as a structurally controlled gold-deposit which is localized by the complex interactions of shearing and folding, producing Z-shaped foliation inflections.

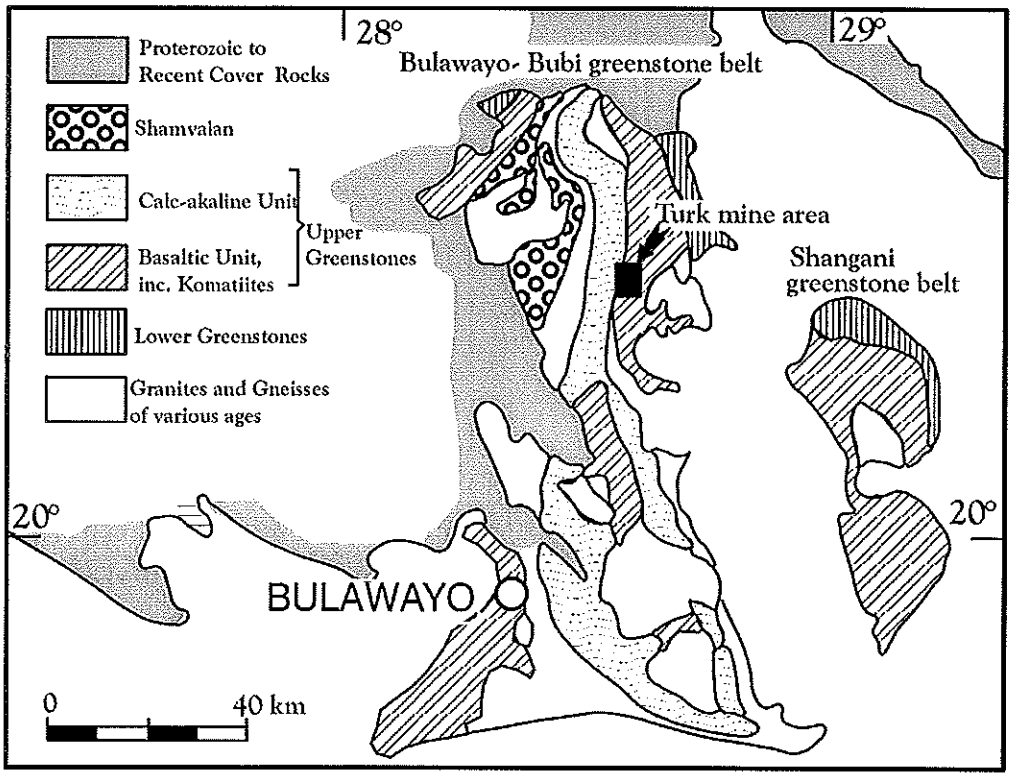

Figure 1: Regional geology of the Bulawayo-Bubi granite-greenstone terrane (modified after Amm, 1940; Macgregor et al., 1937; Wilson, 1979).

Lithologically, the Turk Mine is located within a thick sequence of predominantly mafic volcanics of the Riversbank Group (Riversbank Greenstones), and forms part of the Bembesi gold belt (Macgregor et al., 1937). The mafic volcanics of the Bulawayo-Bubi greenstone belt, which have been dated at 2675 ± 173 Ma (Pb-Pb, Chauvel et al., 1983) and 2690 ± 70 Ma (Rb-Sr, Jahn & Condie, 1976), belong to the lower mafic unit of the western succession of Wilson et al. (1978). The greenstone belts are generally considered to have been developed as fillings of intracratonic basins (e.g. Wilson et al., 1995) or to be generated in a continental margin-type environment (Jelsma et al., 1996). The Turk Mine occurs to the east of a major shear zone, the Gabriella Mulungwane deformation zone, which also acts as an unconformity between the mafic volcanics and a predominantly volcaniclastic sequence of intermediate composition (Fig.2). As described by Campbell & Pitfield (1994) the mine is situated in a relatively narrow intrashear corridor of basaltic rocks on either side of which occur significant strain gradients.

A major, irregular-shaped, quartz-feldspar porphyry intrusion with a north-striking contact to the mafic volcanics occurs about 500 m to the east of the mine (Fig. 2). This intrusion is probably linked to the 2.7 Ga syn- to late-tectonic Sesombi suite of granitiods of Wilson et al. (1978). The contact is further marked by a distinct sedimentary sequence consisting of locally folded and sheared iron formation and dolomitic limestone-breccias (including stromatolites, Macgregor, 1940). The mafic volcanics are overlain by a sequence of predominantly volcaniclastic rocks of intermediate composition. In the mine area these rocks are exposed as agglomerates. Two major dolerite dykes occur at Turk Mine: the hangingwall dyke to the east

(probably located at the footwall) and the crossdyke to the north, which separates the Turk section from the Angelus section 200 m further to the east.

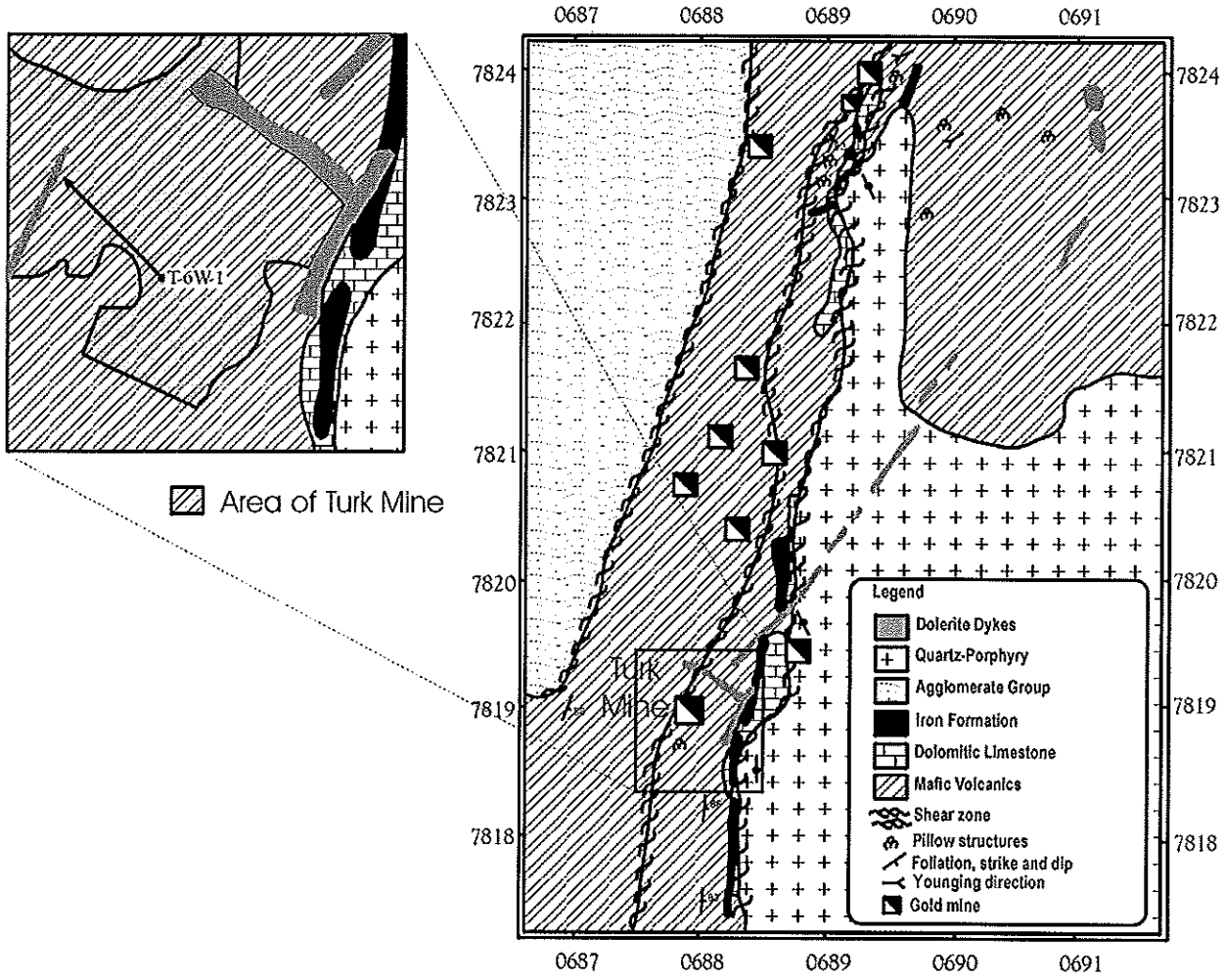

Figure 2: Geological map of the area surrounding Turk Mine indicating the location of borehole T-6W-1.

PETROGRAPHY OF THE WALL ROCK

The mafic volcanics of the Riversbank Group (Macgregor et al., 1937), in which all gold mines of the Bembesi gold belt occur, are divided into three major units:

(1) the undeformed country-rock to the east of the Turk Mine is a commonly pillowed, subophitic-textured and moderately altered metabasalt. Actinolite and subordinate chlorite present in the rock indicate greenschist-facies metamorphism. Zoisite is developed as fine-grained, hypidiomorphic crystals which commonly form aggregates. Euhedral, rhomboidal-shaped porphyroblasts of actinolite embedded within the matrix make up less than 5 vol. % of the rocks. The hydrothermal overprint is usually characterized by a pervasive carbonatization and chloritization of the fine-grained matrix-minerals and actinolite porphyroblasts. Carbonate occurs

as irregular spots surrounded by chlorite. The randomly orientated plagioclase laths are usually less altered;

(2) the intrashear corridor is marked by the occurrence of competent, lens-shaped bodies of undeformed metabasaltic and volcaniclastic rocks, which are embedded within the thick sequences of ultramylonite (unit 3, Table 1). These rocks are generally well preserved and mineralogically very similar to the metabasaltic rocks east of the shear zone. The volcaniclastic rocks are characterized by the occurrence of Ti-magnetite, which has grown at the expense of hornblende. Consequently, the hydrothermal alteration and subsequent gold mineralization are interpreted to be the products of greenschist-facies processes; and,

(3) the gold-deposit at the Turk Mine is situated in a sequence of highly sheared and recrystallized metabasalts, several hundred metres thick, in which the original mineralogy has been completely replaced by varying proportions of carbonate, chlorite, quartz, sericite, leucoxene and sulphide minerals (the sulphides consist of more than 95 vol.% pyrite). The mineral content varies on a cm-scale which might reflect source-rock heterogeneities. Most rocks are (ultra-)mylonitic. While quartz occurs exclusively in veins and stringers (extensional veins), the chloritization and carbonatization are pervasive and can also be observed on a regional scale. Pervasive sericitization seems to be restricted to local structures within the deformed metabasalts. The gold-bearing horizons are mineralogically indistinguishable from their wall rocks. Petrographical investigation has shown further that all alteration minerals can be subdivided into at least two texturally different generations. Compared to the metabasalts in the eastern part of the mine the (ultra-) mylonites lack characteristic metamorphic minerals such as epidote, zoisite and plagioclase. The most common sulphide mineral is pyrite, which is developed as euhedral crystals or occurs in aggregates associated with the chloritization. Arsenopyrite is a minor sulphide phase (Campbell & Pitfield, 1994). Two generations of pyrites can be distinguished. The occurrence of asymmetric pressure fringes appears to be restricted to an older pyrite generation, which is further characterized by a coarsely crystalline texture (up to one cm in diameter). A younger pyrite generation is fine-grained and seems to have originated in secondary microstructures within the mylonites. Observations in the Turk Mine appear to confirm this finding, since the highly sheared and altered metabasalts, with finely disseminated sulphides, generally show higher gold concentrations than those with coarser-grained pyrites (Nelson, pers.commun., 1997). Micro-inclusions of gold have been identified in pyrites of the younger generation.

Detailed investigation of the geology of the area around the Turk Mine (Dziggel, 1998) have shown that while the major hydrothermal alteration, such as chloritization and carbonatization occur on a regional scale, the sericitization is restricted to local structures within the highly deformed metabasalts.

Table 1 : Summarized petrographic characteristics of the Turk Mine deposit and wall rocks

unit	metamorphic minerals	average mineral content (estimated)
1. Undeformed country rock	present	[a]CARBONATE, CHLORITE, PLAGIOCLASE, [b]quartz, pyrite, actinolite, zoisite, epidote
2. Mafic lenses within unit 3	present	[a]CARBONATE, CHLORITE, PLAGIOCLASE, [b]quartz, pyrite, Ti-magnetite, zoisite, epidote
3. (Ultra-) mylonites[c]	not present	[a]CARBONATE, CHLORITE, SERICITE, QUARTZ, [b]pyrite, leucoxene, graphite, hematite, talc

[a] Minerals which commonly form > 10 vol. % of the average mineral content, the sericite-content shows the highest variations ranging from 0-65 vol. % and therefore, is not necessarily associated with mylonitisation and gold-mineralization

[b] Minerals which commonly form < 10 vol. % of the average mineral content in decreasing order

[c] Including orebodies

GEOCHEMISTRY

Sampling and Analytical Procedure

Samples from all lithological units collected in the field around the Turk Mine and from drillcore T-6W-1 (Fig. 3) were analysed for major and trace-element contents by standard X-ray fluorescence techniques (XRF) utilizing the facilities in the Department of Geology, University of the Witwatersrand, Johannesburg. The analytical precision is better than 3 % for major elements and approximately 5 to 10 % for trace elements. The geochemical investigation took into account 67 samples from a section through the undeformed pillow basalts in the footwall to the east of Turk Mine, the highly altered and in parts gold-bearing (ultra-) mylonites, and a sedimentary succession in the hangingwall (Fig.4). Fourteen additional samples were analysed for As, S, Mo, Sb, Ag and Bi by standard XRF techniques at the University of Bremen. All these elements, except for As and S, show concentrations below their detection limits. The gold content of 178 samples from drillcore T-6W-1 was determined by standard assay techniques employed by Casmyn Mining at Turk Mine.

Results

In Figure 4 some selected elements are plotted against the drillcore-depth. In addition, the gold-enriched horizons within the sheared metavolcanics are shown. As can be seen from the diagram the strongest variations in element concentrations occurs in a zone between 50-70m away from the mineralized mylonites. Within the sheared metavolcanics none of the elements

show any (negative or positive) correlation with Au. Furthermore, the contact between the metabasalts in the footwall and the mylonites is not marked by any significant geochemical changes. In contrast, the highly incompatible elements Rb, K and Ba have their lowest concentrations in a zone within the shear zone comprising all gold-enriched horizons in the drillcore. The highest concentrations of these elements can be observed on either side of this zone of relative depletion suggesting that the concentration of LIL-elements is directly controlled by the gold mineralizing process. This finding is interpreted to be due to a change in the geochemical composition of white mica in the rocks (paragonite, Roth, pers. commun., 1997), because the highest abundance of white mica occurs within this zone of relative Rb, K and Ba depletion.

In Figure 5 the concentrations of arsenic and sulphur (14 samples) are plotted against drillcore-depth. The gold concentrations and the calculated correlation coefficients (r) of the samples are also shown. In general, the As- and S-enrichment show highly significant correlation with gold concentration. Away from the shear zone, the concentrations of these elements range around zero.

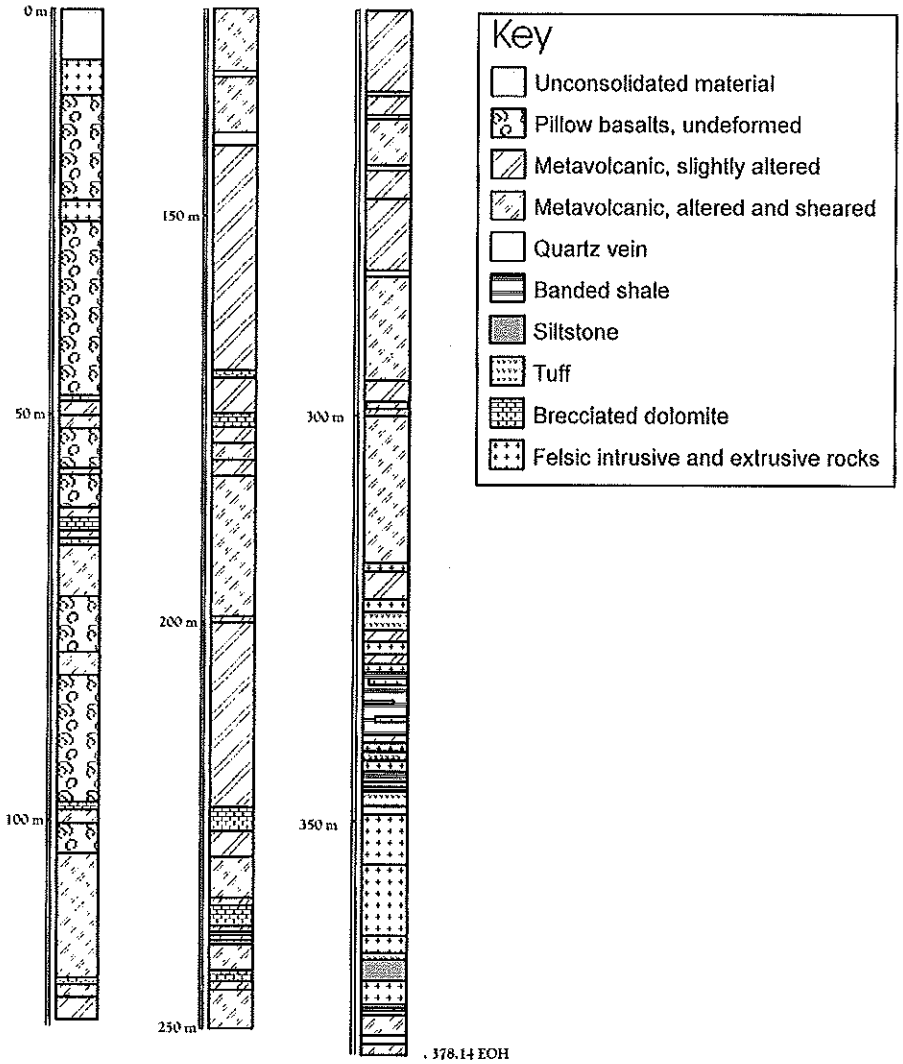

Figure 3: Log of borehole T-6W-1.

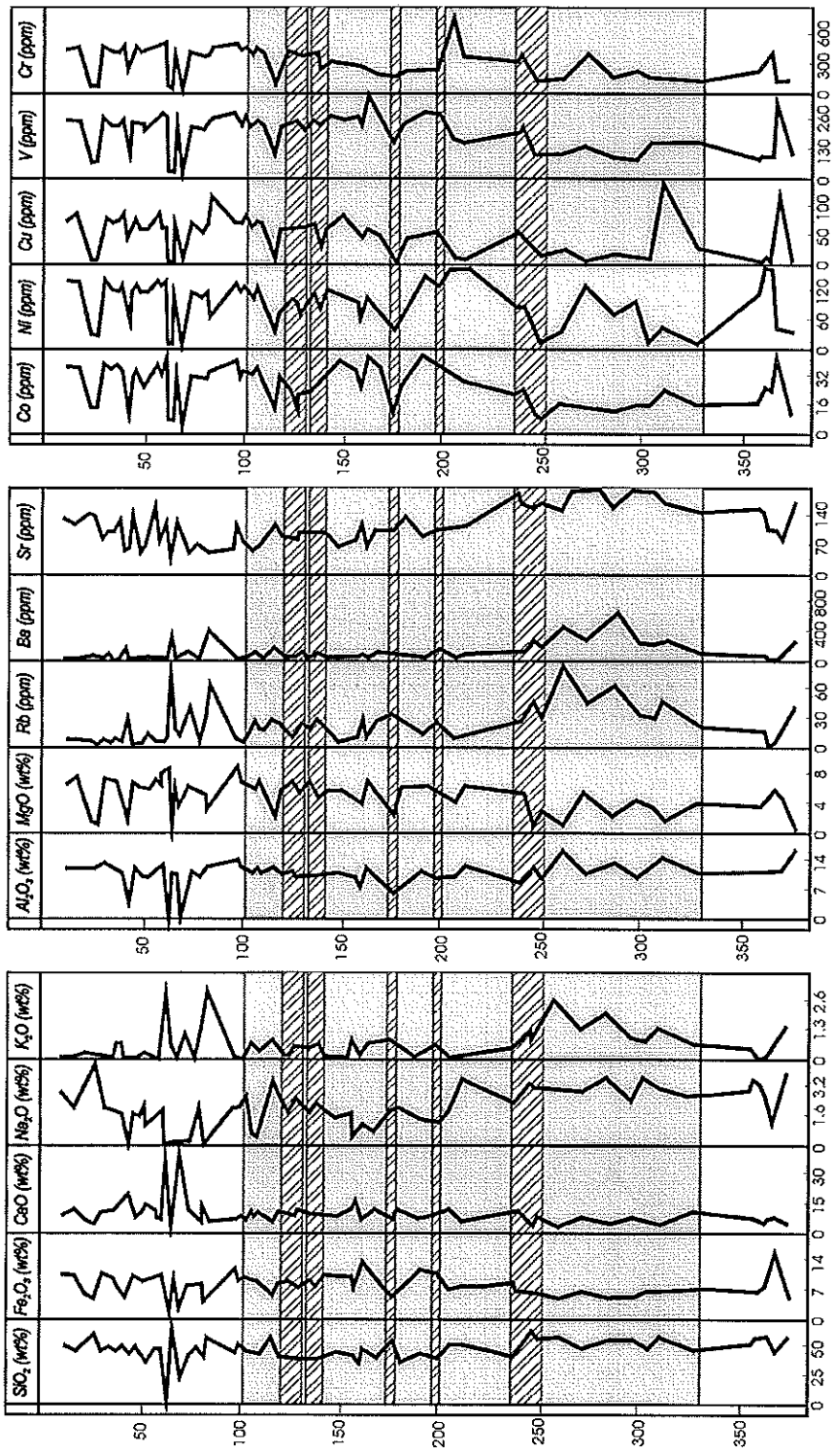

Figure 4: The distribution of selected major and trace elements in borehole T-6W-1 plotted against depth. The horizontal scale represents depth in metres, the vertical scales represent concentrations of oxides and elements in wt% and ppm respectively. The grey shaded area represents the zone of shearing, the hatched areas represent zones of increased gold abundance. The average gold concentrations in these horizons are (with increasing depth) horizon 1 = 1.5ppm; horizon 2 = 3.45 ppm; horizon 3 = 10.31 ppm; horizon 4 = 8.4 ppm; horizon 5 = 3.2 ppm.

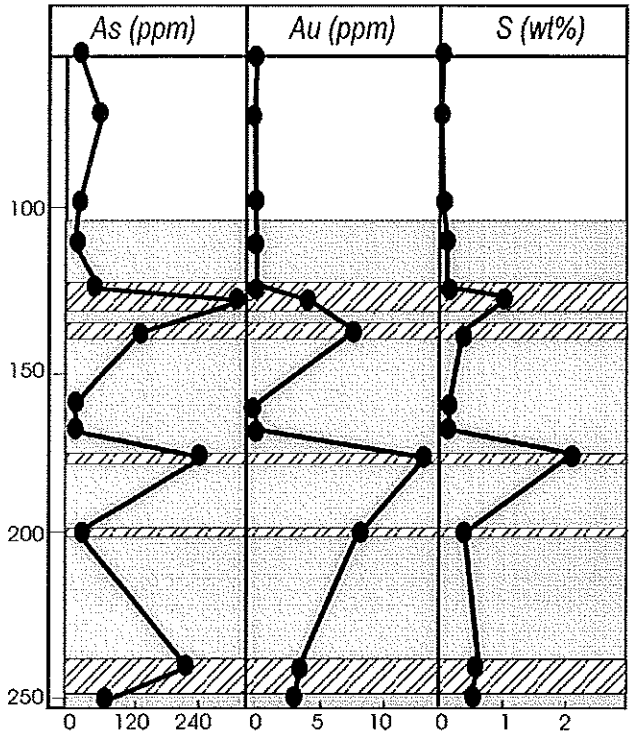

Figure 5: The distribution of arsenic, sulphur and gold in selected samples from borehole T-6W-1. The significance of the shaded and hatched areas is identical to that in Figure 4. Borehole depth (m) is plotted on the vertical axis, elemental concentration on the horizontal axis.

STATISTICAL ANALYSIS

In order to further investigate the interrelationships between gold mineralization and the hydrothermally overprinted wall rocks, a statistical manipulation of the data was undertaken. The distribution of gold in the altered wall rocks is characterized by a mean value of 0.2 ppm. The economically important mineralization from drillcore T-6W-1 has average concentrations of about 3 ppm. For comparison, the gold contents of some Archaean greenstone belts elsewhere in southern Africa range between 0.1-372 ppb with an arithmetic mean gold content of 10.8 ppb (Saager et al., 1982). The petrographic and geochemical data from this study imply that the orebodies and the altered wall rocks (both being mylonites) are indistinguishable, except on the grounds of gold content.

Results

The frequency distribution of the gold concentration data is positively skewed, which is indicative of a lognormal distribution. This is supported by a non-parametric Kolmogorov Smirnov test which demonstrates that the d- value (0.071) does not exceed the critical value at a 0.0001 significance level. All samples collected from drillcore T-6W-1, between 47.5- 302.48 m , show an arithmetic mean Au content of 1.053 ppm ranging between the detection limit (0.02 ppm) and 13.7 ppm. The geometric mean, which is commonly a better measure than the arithmetic mean, has a value of 0.19 ppm. When logarithmically transformed, the data do not

exhibit a perfectly normal distribution but indicate an overlap of two different (lognormally distributed) populations. The histogram is double-peaked.

The cumulative frequency distribution does not yield a straight line, but defines a line with one inflection point, which also indicates two overlapping populations in the data set. Following Lepeltier (1969) such a graph is the expression of a dual distribution where the central branch represents a mixture of both populations. Separating these two populations, by employing the graphical partitioning method described by Sinclair (1978), it was found that 72.5 % belong to a background population and 27.5 % belong to an excess value population (termed by Lepeltier, 1969, Fig.6), if the threshold value for the background population is set at $\bar{x}_B - 2s = 0.66$. Population A has an arithmetic mean of 0.08 ppm and population B shows an arithmetic mean gold content of 2.7 ppm.

In the following section a statistically useful connection between gold-distribution and the geochemistry of the altered wall rocks was calculated by employing the discriminant analysis (e.g. Swan & Sandilands, 1995).

For this multivariate approach the samples were separated into two groups: rocks with gold contents < 0.1 ppm were placed into group 1, and all samples with more than 0.1 ppm gold were allocated to the second group. The discriminant function, which maximizes the distance between the vector means of these groups, was subsequently calculated on the basis of all other geochemical results (23 variables).

As shown in Table 2, 10 out of the 23 variables were found to be suitable to discriminate between the previously defined groups. The result is highly significant ($p = 0.0002$). Thus, it is possible to recalculate the group membership for each case using the discriminant function. Detailed information about the statistical terms used in Table 2-4 can be obtained from suitable software packages, e.g. STATISTICA (StatSoft, Inc. 1995).

Table 2 : Variables which are statistically suitable for discriminating between mineralized and unmineralized samples. The result is statistically highly significant (p= 0.0002)

STAT.	Discriminant Function Anaysis Summary (pro2.sta)					
DISCRIM.	Step 10, N of variables in model: 10; Grouping: GROUP-AU (2 groups)					
ANALYSIS	Wilks' Lambda: .15185 approx. F (10,15) = 8.3781 P < 0.0002					
N = 26	Wilks' Lambda	Partial Lambda	F-remove (1.15)	p-level	Toler.	1-Toler.
Wt% TiO_2	0.250964	0.605069	9.79005	0.006896	0.048575	0.951425
LOG Rb	0.457817	0.331684	30.22374	0.000061	0.081525	0.918475
Wt% P_2O_5	0.157374	0.964905	0.54558	0.471531	0.212846	0.787154
LOG Na_2O	0.405756	0.374241	25.08115	0.000156	0.136325	0.863675
PPM Zn	0.351097	0.432503	19.68188	0.000481	0.122502	0.877498
PPM Zr	0.242025	0.627416	8.90760	0.009259	0.046902	0.953035
PPM Y	0.247351	0.613907	9.43365	0.007757	0.051902	0.948098
LOG Nb	0.201285	0.754405	4.88322	0.043082	0.104905	0.895095
LOG Sr	0.176157	0.862007	2.40125	0.142076	0.268501	0.731499
Wt% MgO	0.168087	0.903407	1.60381	0.224677	0.268305	0.731695

The variables entered into the model are characterized by a high discriminatory power (Wilks'Lambda = 0.15). In general this value is the standard statistic used to denote the statistical significance of the discriminatory power of the model. Its value ranges from 1.0 (no discriminatory power) to zero (perfect discriminatory power). The results in Table 2 show further that none of these variables are marked by a high discriminatory power. The values for the partial Lambda, which defines the unique contribution of the respective variable to the discrimination between groups, range between 0.33-0.90. Table 3 shows the standardized discriminant function coefficients. The discriminant function seems to be marked mostly by the variables TiO_2 and Y, the contribution of all other variables being less than half that for these elements.

Table 3 : Standardized coefficients of the discriminant function

STAT. DISCRIM. ANALYSIS	Standardized Coefficients for Canonical Variables
Variable	Root 1
Wt% TiO_2	-3.09611
LOG Rb	3.10891
Wt% P_2O_5	0.44092
LOG Na_2O	2.32637
PPM Zn	2.33708
PPM Zr	-3.05835
PPM Y	2.96154
LOG Nb	-1.66141
LOG Sr	-0.77843
Wt% MgO	-0.65151
Eigenval	5.58542
Cum. Prop.	1.00000

In order to test the suitability of the calculated discriminant function the Mahalanobis distances were calculated. These are a measure of the distance that can be used in a multivariate space defined by the variables in the model for each case. The level of confidence increases with decreasing distance of each case value to a group centroid. As shown in Table 4, the calculated discriminant function works with a high accuracy, considering the fact that these are all post-classifications. From a statistical point of view this means that the maximum distance between the two mean vectors of the previously defined groups is large enough to assign each case (sample) to the correct group using the Mahalanobis distances. Therefore, the discriminant function can be used as a tool to evaluate which samples have high or low gold concentrations, respectively.

The product moment correlation coefficient matrix was calculated for 13 variables (Table 5). A Kolmogorov Smirnov test was applied to all elements and, consequently, the Rb, Ba, Ca, LOI and Au data have been logarithmically transformed.

Table 4 : Squared Mahalanobis distances from group centroids

STAT. DISCRIM. ANALYSIS	Squared Mahalanobis Distances from Group Centroids (pro2.sta)		
Case	Observed Classif.	Void p = 0.57692	Rich p = 0.42308
T-6W-1-10	Void	4.8997	25.93655
T-6W-1-18	Void	19.32487	34.30194
T-6W-1-19	Void	8.26569	14.55393
T-6W-1-23	Void	10.72367	37.14739
T-6W-1-28	Void	4.79477	25.08595
T-6W-1-29	Void	11.33228	36.01372
T-6W-1-31	Void	1.96304	23.22815
T-6W-1-32	Rich	23.43270	4.16690
T-6W-1-33	Rich	10.70179	5.43367
T-6W-1-35	Void	7.16370	46.45304
T-6W-1-36	Void	6.90199	20.18642
T-6W-1-37	Void	16.89650	56.87791
T-6W-1-39	Void	7.62420	23.24372
T-6W-1-40	Rich	35.81957	12.83275
T-6W-1-41	Void	7.75184	11.17996
T-6W-1-43	Rich	24.58119	7.65849
T-6W-1-44	Void	14.41545	44.86353
T-6W-1-46	Rich	37.23061	5.92118
T-6W-1-47	Rich	28.66123	11.49854
T-6W-1-48	Rich	41.31042	15.82032
T-6W-1-49	Void	11.72696	38.54682
T-6W-1-51	Void	9.09207	22.10368
T-6W-1-59	Rich	31.80558	8.85848
T-6W-1-60	Rich	24.31227	3.77869
T-6W-1-61	Rich	32.89467	8.31560
T-6W-1-62	Rich	38.72677	12.83851

Table 5 : Correlation matrix for the geochemical data from samples collected from drillcore T-6W-1. Statistically significant correlations are marked with an *

Variable	SiO_2	TiO_2	Al_2O_3	Fe_2O_3	MnO	MgO	K_2O	P_2O_5	log.Rb	log.Ba	log.Ca	log.LOI
log. Au	0.16	-0.19	-0.06	-0.12	-0.35	-0.21	0.29	-0.26	0.38*	0.32	0.24	0.15
log. LOI	-0.82*	-0.37	-0.74*	-0.13	0.62*	0.25	-0.25	-0.47*	-0.05	-0.22	0.78*	1.00
log. CaO	-0.86*	-0.26	-0.72*	0.11	0.89*	0.46*	-0.64*	-0.54*	-0.45*	-0.58*	1.00	
log. Ba	0.53*	-0.02	0.23	-0.41*	-0.59*	-0.52*	0.85*	0.53*	0.9*	1.00		
log. Rb	0.34	-0.11	0.12	-0.43*	-0.48*	-0.51*	0.93*	0.26	1.00			
P_2O_5	0.55*	0.30	0.43*	-0.23	-0.51*	-0.38*	0.40	1.00				
K_2O	0.47*	0.03	0.33	-0.39*	-0.60*	-0.56*	1.00					
MgO	-0.56*	0.33	0.09	0.74*	0.49*	1.00						
MnO	-0.86*	-0.13	-0.58*	0.21	1.00							
Fe_2O_3	-0.21	0.77*	0.45*	1.00								
Al_2O_3	0.53*	0.72*	1.00									
TiO_2	0.13	1.00										
SiO_2	1.00											

The highest correlation coefficients were determined for the element-pairs SiO_2,/LOI, SiO_2/CaO, CaO/MgO, K_2O/Ba, K_2O/Rb and MnO/SiO_2. However, appart from Rb (r = 0.38*) none of these elements correlates significantly with gold; the correlation coefficients with all other elements range around zero.

A statistical method supplying information about the number and kind of the geological (or geochemical) processes which are responsible for the total variances of the data set is a (usually varimax rotated) factor analysis. The extracted factor model, listed in Table 6, accounts for about 90 % of the total variances of the original data set (13 variables).

Table 6 : R-mode factor matrix for geochemical data from samples collected from drillcore T-6W-1. For further information see text

variable	factor 1	factor 2	factor 3	factor 4	communalit.
SiO_2 %	0.132686	0.925899	0.230377	-0.029803	0.928856
TiO_2 %	-0.879636	0.231522	0.056872	-0.225441	0.881419
Al_2O_3 %	-0.647470	0.669206	0.174013	-0.114208	0.910378
Fe_2O_3 %	-0.915577	-0.045478	-0.329691	0.090532	0.957241
MnO %	-0.048197	-0.834563	-0.396196	-0.154806	0.879754
MgO %	-0.669782	-0.425039	-0.464933	0.057865	0.848777
K_2O %	-0.077112	0.298904	0.905340	0.036136	0.916236
P_2O_5 %	0.010732	0.491506	0.390856	-0.641789	0.806354
Rb ppm	0.150592	0.101236	0.950605	0.139816	0.956125
Ba ppm	0.127556	0.285003	0.901331	-0.013303	0.910071
CaO %	0.076425	-0.884098	-0.391591	-0.056555	0.944012
LOI %	0.178676	-0.901161	0.035544	0.207565	0.888362
Au ppm	0.103648	0.115593	0.299463	0.879814	0.874355
Expl.Var	2.593314	4.267429	3.448969	1.353544	
%-Prop.	19.95 %	32.83 %	26.53 %	10.4 %	
Prop.Tot l	19.95 %	52.78 %	79.31 %	89.71 %	

The high communality values, which are displayed by all investigated elements, indicate that each of them is explained to more than 80 % by the model. The highest communalities are given for the elements Fe_2O_3 and Rb, while MgO and P_2O_5 show the lowest communalities, respectively. Proportionally, factor 2, with 32. 83 %, ecplains most of the variances, where as factor 4, with 10.4 %, yielded the least variances of the original data set.

Factor 1 possesses a high negative loading of Fe_2O_3, TiO_2 and, to a lesser extent, of MgO. The arithmetic mean of Fe_2O_3 (8 %) of the investigated data set was found to be representative of all analysed samples which display an arithmetic mean of 8.3 %. TiO_2 shows an arithmetic mean of 0.68 % in contrast to 1.9 % of the whole data set, while the arithmetic mean of MgO (5.8 %) is in accordance with the mean content of 5.41 %. The high correlation coefficients of these elements in Table 5 confirms the interrelationship between them. Factor 1 is termed the

"chlorite-factor". The good correlation of TiO_2 with this factor is a reflection of the commonly observed association of chlorite and leucoxene, although the small standard deviation of 2.07 for Fe_2O_3 and 1.72 for MgO in all the samples studied suggest that the concentrations of these elements may be primary in origin (see below). Therefore, factor 1 can also be termed the "mafic-mineral factor".

The highest loadings in **factor 2** are shown by SiO_2, CaO and LOI (0.92, -0.88 and -0.909, respectively). The loss on ignition can be used as a measure for the CO_2-(H_2O) content in the samples, and is therefore used as a measure of the carbonate content with a correlation coefficient of 0.78. SiO_2 and CaO are also highly correlated (r = 0.86). Factor 2 therefore describes two different types of alteration: namely carbonatization and silicification. The negative correlation can probably be put down to the fact that the quartz precipitation in veins and stringers represents a separate by-product of the carbonatization process. The commonly observed association of carbonate and chlorite in the samples suggests that this factor is also responsible for the chloritization. Consequently, the carbonatization, silicification and chloritization may have been a simple carbonatization/hydration process such as:

(1) $3Ca_2(Mg,Fe)_5Si_8O_{22}(OH)_2 + 2Ca_2Al_3Si_3O_{12}(OH) + 10CO_2 + 8H_2O \rightarrow 3(Mg,Fe)_5Al_2Si_3O_{10}(OH)_8 + 10CaCO_3 + 21SiO_2$

Actinolite Epidote Fluid Chlorite Calcite Quartz

Factor 3 is exclusively loaded by the highly incompatible elements Rb, Ba and K. The element contents of Ba and Rb show strong variations around their arithmetic mean of 115 ppm and 29 ppm, respectively. These large variations from 16-471 ppm for Ba and 10-88 ppm for Rb seem to indicate that these elements depend on the sericitization. The following reaction is considered to have taken place:

(2) $3(Mg,Fe)_5Al_2O_{10}(OH)_8 + 15CaCO_3 + 2K^+ + 15CO_2 \rightarrow 2KAl_3Si_3O_{10}(OH)_2 + 15Ca(Mg,Fe)(CO_3)_2 + 3SiO_2 + 9H_2O + 2H^+$

Chlorite Calcite Fluid Sericite Fe-Dolomite Quartz Fluid

Factor 4 is largely loaded by gold alone and is, therefore, termed the "gold-factor". The complete separation of gold from all other elements strongly suggests that there is no

fundamental relationship between the gold-enrichment and the different types of alteration (viz. chloritization, sericitization, carbonatization and silicification. This is important because it indicates that fluid inclusion or stable isotope studies of the altered wall rocks or the quartz veins of the orebodies would not nececarialy give any relevant information on the original P-T-X conditions, or the source, of the gold mineralizing fluid.

DISCUSSION AND CONCLUSIONS

The geochemical characteristics of the Turk Gold Mine give an important insight into the complexity of the structurally controlled geochemical processes which have been associated with the formation of economic gold deposits. In contrast to many other lode-gold deposits the petrography, geochemistry and the different statistical methods used in this study show unequivocally that the economic gold enrichment at the Turk Mine is not directly correlated with silicification and carbonatization or any other type of alteration. Furthermore, the formation of this gold deposit postdates the different activities of pervasive fluid migration and subsequent wall-rock alteration. Since most lode-gold deposits in Zimbabwe and elsewere are developed as massive quartz veins, this investigation shows further that structurally controlled fluid migration, which results in the formation of quartz veins, is not necessarily associated with the formation of economic gold mineralization nor can it be used as a pathfinder. The factor analysis illustrates that at least two different geochemical processes have been preserved in the highly deformed country rock prior to the emplacement of the gold mineralization. These processes comprise the hydration and carbonatization of the mafic minerals and a subsequent potassium metasomatism, which might have been related to an earlier stage of the tectonic evolution of the greenstone belt. Since one gold deposit occurs within the syn- to late-tectonic quartz-feldspar-porphyry to the east of Turk Mine, it is suggested that the gold mineralization may predate, or be synchronous with, the main phase of the tectonic activity.

ACKNOWLEDGEMENTS

The authors wish to thank Casmyn Mining, Zimbabwe, for access to sample material and related information, as well as for their generous hospitality and logistical support at Turk Mine. We also gratefully acknowledge support for this research by the Foundation for Research Development and by the University of the Witwatersrand.

REFERENCES

Amm FL (1940) The geology of the country around Bulawayo. Southern Rhodesian Geological Survey Bulletin No. 35, 270 pp.

Blenkinsop T, Martin A, Jelsma HA, Vinju ML (1997) The Zimbabwe Craton. In: De Wit MJ, Ashwal LD (eds.) Greenstone Belts. Oxford Monographs on Geology and Geophysics 35: 567-580.

Boyle RW (1979) The geochemistry of gold and its deposits. Geol Surv Can Bull 280: 584 pp.

Campbell SDG, Pitfield PEJ (1994) Structural controls of gold mineralisation in the Zimbabwe Craton, exploration guidelines. Bull Geol Surv Zimb 101: 270 pp.

Chauvel C, Dupré, B, Todt W, Arndt ND, Hoffmann AW (1983) Pb and Nd isotopic correlation in Archaean and Proterozoic greenstone belts, Rhodesia. Earth Planet Sci Lett 27: 155-162.

Colvine AC, Fyon JA, Heather, KB, Marmont S, Smith PM, Troop, DG (1988) Archaean lode gold deposits in Ontario. Ontario Geol Surv Misc Paper 139: 136 pp.

Dziggel A (1998) Geologische und Geochemische Untersuchungen der archaischen Goldlagerstätte Turk Mine, Bulawayo-Bubi Greenstone Belt, Zimbabwe. Unpubl Diplomarbeit, Universität Bremen: 165 pp.

Foster RP (1989) Archaean gold mineralisation in Zimbabwe: implications for metallogenesis and exploration. Econ Geol Mon 6: 54-70.

Garson MS, Fimm FGS (1995) The geology of the Bulawayo greenstone belt and the surrounding granitic terrain. Bull Geol Surv Zimb 93: 294 pp.

Groves DI (1993) The crustal continuum model for late-Archaean lode-gold deposits of the Yilgarn Block, Western Australia. Mineral Deposita 28: 366-374.

Jahn BM, Condie KC (1976) On the age of Rhodesian greenstone belts. Contrib Mineral Petrol 57: 317-330.

Jelsma HA , Vinyu M, Valbracht P, Davies G, Wijbrans J, Verdurmen E (1996) Constraints on Archaean crustal evolution of the Zimbabwe Craton: a U-Pb zircon, Sm-Nd and Pb-Pb whole rock isotope study. Contrib Mineral Petrol 124: 55-70.

Lepeltier C (1969) A simplified statistical treatment of geochemical data by graphical representation. Econ Geol 64: 538-550.

Macgregor AM (1940) A Precambrian algal limestone in Southern Rhodesia. Trans Geol Soc S Afr 43: 9-16.

Macgregor AM, Ferguson JC, Amm FL (1937) The geology of the country around Queen's Mine, Bulawayo District. Bull Geol Surv Rhod 30: 175 pp.

Phillips GN, Groves DI (1984) Fluid access and fluid-wall rock interaction in the genesis of the Archaean gold-quartz vein deposit at Hunt Mine, Kambalda, Western Australia, In: Foster RP (eds.) Gold `82: Rotterdam, AA Balkema: 337-359.

Saager R, Meyer M, Muff R (1982) Gold distribution in supracrustal rocks from Archaean greenstone belts of southern Africa and from Palaeozoic ultramafic complexes of the European Alps: metallogenic and geochemical implications. Inform Circ Econ Geol Res Unit Univ Witwatersrand, Johannesburg 156: 26 pp.

Sinclair AJ (1978) Applications of probability graphs in mineral exploration. Spec Vol Assoc Expl Geochemists 4: 95 pp.

Statsoft, Inc. (1995) Statistica for windows [computer program manual]. Tulsa, OK: Statsoft, Inc., 2325 East 13th Street, Tulsa, OK 74104 .

Swan ARH, Sandilands M (1995) Introduction to Geological Data Analysis. Blackwell Science: 446 pp.

Wilson JF, Bickle MJ, Hawkesworth CJ, Martin A (1978) Granite-greenstone terrains of the Rhodesian Archaean craton. Nature 271: 23-27.

Wilson JF (1979) A preliminary reappraisal of the Rhodesian Basement Complex. Spec Publ Geol Soc S Afr 5: 1-23.

Wilson JF, Nesbit RW, Fanning CM (1995) Zircon geochronology of Archaean felsic sequences in the Zimbabwe Craton: a revision of greenstone stratigraphy and a model for crustal growth. In: Coward MP, Ries AC (eds.) Early Precambrian Processes. Geol Soc Lond Spec Pub 95: 109-126.

_____oOo_____